

## Efficient simulation of wildfire spread on an irregular grid

Paul Johnston<sup>A,B</sup>, Joel Kelso<sup>A</sup> and George J. Milne<sup>A</sup>

<sup>A</sup>School of Computer Science and Software Engineering, University of Western Australia, M002, 35 Stirling Highway, Crawley, WA 6009, Australia.

<sup>B</sup>Corresponding author. Email: paulj@csse.uwa.edu.au

**Abstract.** A cell-based wildfire simulator that uses an irregular grid is presented. Cell-based methods are simpler to implement than fire front propagation methods but have traditionally been plagued by fire shape distortion caused by the fire only being able to travel in certain directions. Using an irregular grid randomises the error introduced by the grid, so that the shape of simulated fire spread is independent of the direction of the wind with respect to the underlying grid. The cell-based fire spread simulator is implemented using discrete event simulation, which is a much more efficient computational method than conventional wildfire simulation techniques because computing resources are not used in repeatedly computing small updates to parts of the fire whose dynamics change infrequently, namely those areas of a fire that move slowly. The resulting simulator is comparable in accuracy with traditional fire front propagation schemes but is much faster and can therefore be used as an engine for fire simulation applications that require large numbers of simulations, such as in the role of a risk analysis engine.

**Additional keyword:** discrete event simulation.

### Introduction

Wildfire spread is governed by several physical processes. The processes involved in the spread of a wildfire include heat generation by combustion, consumption of heat by evaporation and volatilisation and heat transfer by conduction, convection, radiation and solid mass transport (spotting). A complete physical understanding of these processes and their relative importance in grass and forest fires is lacking owing to the difficulty in conducting experiments under the range of conditions experienced in nature or collecting accurate data during wildfires. Computational simulation of the physical processes is also difficult owing to the range in length scales on which they operate, and the complex nature of fire caused by turbulence of the atmosphere during a fire. Furthermore, there exist the inherent problems of collecting sufficient accurate input data that describes the natural environment, and to keep those data up to date owing to growth of plants and changes in moisture caused by rainfall and weather changes. Additionally, numerical integration of the physical equations requires enormous computational resources (e.g. Linn *et al.* 2002).

Despite our incomplete physical understanding of the processes governing fire spread, statistical relationships between the macroscopic factors that affect the spread of wildfire and fire behaviour can be used in forecasting fire spread over the landscape. Fire behaviour experiments and wildfire observations show that the most important factors governing the macroscopic rate of spread are wind speed, fuel moisture and slope of the terrain (e.g. McArthur 1967). These relationships, called fire behaviour models, are approximate in nature and there is a large degree of variance in the observed rate of spread under similar conditions even for well-controlled experiments. This is thought to be due to variation in the wind speed experienced at the level of

the fire and inaccuracy in the estimation of fuel moisture. Therefore, more precise measurement of the wind field (Sullivan and Knight 2001) and live and dead fuel moisture (e.g. Matthews 2006) are the objects of ongoing research. Other factors, such as the width of the fire front, influence the forward rate of spread of fire (Cheney and Gould 1995) and contribute to the variability seen in the relationship between the observed and predicted fire behaviour if these factors are not included in the fire behaviour model.

These empirical fire behaviour models are more readily implemented into computational simulation models than direct modelling of the physical process (e.g. Linn *et al.* 2002) and there is a long history of fire spread simulators that incorporate empirical fire behaviour models into a system for the prediction of the spatial spread of fire (e.g. Kourtz and O'Regan 1971; Coleman and Sullivan 1996; Finney 1998; CWFGM Project Steering Committee 2004; for recent reviews, see Pastor *et al.* 2003; Sullivan 2008). Two quite different approaches have been used to implement empirical fire spread simulation. Cell-based methods divide the landscape into small discrete areas called cells (usually squares or hexagons) and determine the time that each cell on the landscape ignites (e.g. Green Tridgell *et al.* 1990). For surface fires, the delay between ignition of a cell and its neighbours is determined by the distance between cells divided by the rate of spread in the direction of the neighbour. In contrast to this cell-based approach, front propagation methods model each fire as a continuous curve on the landscape that is propagated outwards at the rate of spread determined by the fire behaviour model at discrete points on the curve (e.g. Finney 1998). Earlier wildfire simulators often adopted the cell-based approach because of the ease with which it can be implemented. This method has fallen out of favour largely because of distortions of the fire shape that

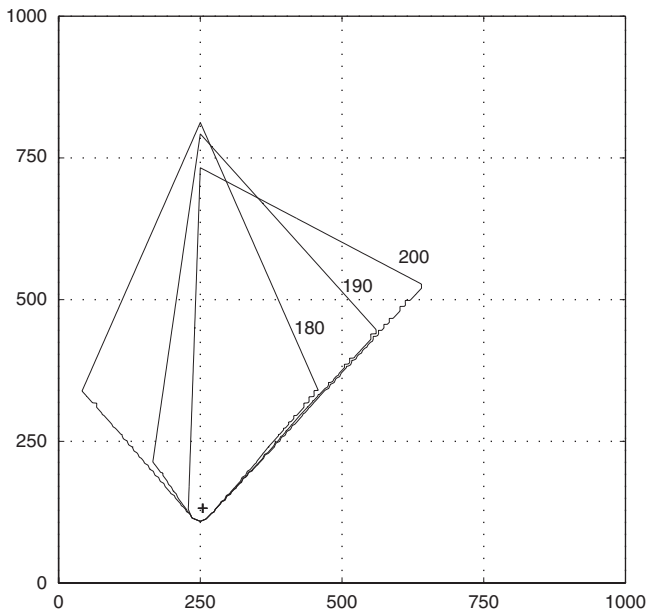


**Fig. 1.** Fire position calculated with a cell-based simulator on a regular eight-neighbour grid after 30 min for a point ignition where the head fire rate of spread is  $1000 \text{ m h}^{-1}$  and the flank fire rate of spread is  $31 \text{ m h}^{-1}$ . The fire shape is shown for three different wind directions ( $180$ ,  $190$  and  $200^\circ$ ) with the same ignition location marked with a plus sign (+). The shape of the fire is angular and varies strongly with wind direction, and the maximum spread direction is always aligned with the underlying grid.

are caused by grid geometry (e.g. Kourtz and O'Regan 1971). Front propagation methods avoid this problem because the discrete points on the fire front are not tied to any underlying grid. Over the last 10 to 15 years, improvements in the algorithms that implement the front propagation method have aimed to improve the realism of these simulations, for example to ensure that the fire front does not overlap itself, and to ensure the removal of internal fire fronts when they burn out a patch of unburnt fuel (Richards 1999).

As mentioned above, the main reason that cell-based simulators are not more widely used is because of the distortion of the fire shape they produce; they do not faithfully predict the correct rate of spread in all directions as shown in Fig. 1. In fact, for cell-based simulations on a regular grid, the simulated fire shape varies as a function of the wind direction with respect to the underlying grid and the maximum spread occurs along the grid direction closest to the wind direction. Yet cell-oriented simulation methods are attractive owing to their potential for high performance, allowing large-scale detailed simulations to be performed rapidly. In the present paper, we address the underlying problem of regular gridded cell-based simulation, so permitting the computational efficiency of this approach to then be exploited. We present a novel cell-based approach designed to minimise the distortion of fire shape caused by the underlying grid by employing an irregular grid, so that the directions of the immediate neighbouring cells of a given cell are different from those of any other cell. The use of this irregular grid technique necessarily introduces some error by allowing the fire to travel in only a finite set of directions at the fine scale, and we describe

in the present paper the technical issues arising from the use of an irregular grid and how these are solved. However, we demonstrate that over time the discretisation errors average out rather than accumulate as they do for a regular grid.

We are able to implement an irregular grid for simulation of fire behaviour by explicitly modelling cell location and the connectivity network between cells. The direction of the links connecting cells is used in calculating the rate of spread of fire along those links. We also adopt a discrete event simulation methodology (Zeigler 1984) to achieve an extremely efficient means of propagating the fire over the landscape. In a discrete event simulation, all ignitions, weather and fuel state changes are modelled as events. This method is more efficient than a fire front propagation method because in the discrete event method, the fire front advances by the size of a cell at each ignition event, whereas in a fire front propagation method, a large number of small steps in the fire front require repeated calculation, even for the slow-moving parts of the fire front. Also, because of the simplicity of the cell approach, there is no checking required to ensure that the simulation does not reach an infeasible state (such as the fire line overlapping itself). This increase in speed combined with propagation of the fire front at the correct rate of spread in all directions results in a fire simulator that is as accurate as the fire front propagation simulators with additional performance advantages. This high-performance simulation engine will be useful for applications that require multiple simulations of the same fire like *FSPPro* (McDaniel 2007) or of many different fires for fire-season planning, and will allow these types of simulations to be run with relatively modest computing resources.

## Materials and methods

In this section, we present the theory underlying the cell-based method of simulation of wildfire. Although this theory is well known, we give a complete presentation in order to show that it is not necessary to assume that the spatial structure of the cells is regular, nor is it necessary to update the states of all cells simultaneously as occurs in front propagation and classical synchronous update cellular automata approaches (e.g. Berjak and Hearne 2002).

### Cells

The cell-based method of simulation of wildfire divides the landscape into cells, usually but not necessarily of equal shape and area, creating a network structure of interconnected cells. The state of each cell contains information about that part of the landscape that it represents, namely:

- a cell identifier,
- map location,
- a list of its neighbouring cells,
- the fuel parameters required by the fire behaviour model (usually fuel load, fuel moisture, vegetation type),
- slope and elevation,
- fire state (unburnt, ignited),
- wind speed and direction.

The behaviour of each cell is modelled by a transition function that models interaction between cells, namely the spread of

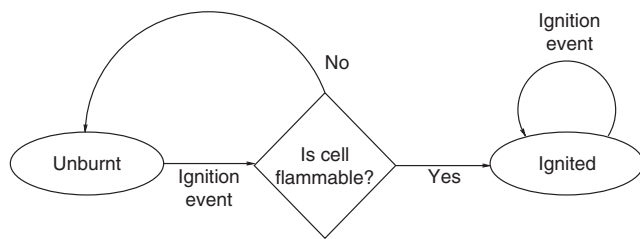


**Fig. 2.** The fire state of a cell and how state changes in response to an ignition event. The ellipses represent the two fire states unburnt and ignited. When an unburnt cell receives an ignition event, the fuel state and fire behaviour model are used to determine if ignition occurs. Ignition events for already ignited cells are ignored.

ignition events that modify the fire state of neighbouring cells. The collective fire state for the entire landscape captures the progress of the simulated fire through time.

### Events

Changes in cell properties occur via events. The most important event type in a fire spread simulator is the ignition event. As shown in Fig. 2, a cell in the unburnt state that receives an ignition event changes state to ignited if its fuel type allows it (i.e. it contains fuel and the fuel moisture is below the extinction fuel moisture). Receipt of an ignition event by a cell in an ignited state has no effect. Other events in the model may modify the cell's fuel moisture or the wind speed and direction. If we assume that the weather is the same across the entire landscape being modelled, then a change in fuel moisture for a given fuel type applies to all cells that contain that fuel type and a global array of fuel moisture values corresponding to all the fuel types in the landscape can be updated, rather than updating the fuel moisture in each cell. Similarly, a single global wind vector can be applied to the entire landscape if we assume spatially uniform wind speed. Relaxing either of these assumptions is straightforward – in that case, the wind and fuel moisture states would be stored for each cell and could therefore vary spatially.

### Propagation delay

So far, we have discussed the behaviour of a cell in isolation from the other cells in the model. We are able to do this because we have formalised the interaction between cells via events and the source of the event does not change the behaviour of the cell. In practice, to simulate surface fire, we only allow cells to trigger ignition events in their immediate neighbours some time after the cell enters the ignited state. We call the time delay between ignition of a cell and the triggered ignition event of its neighbour the propagation delay. This concept is demonstrated in Fig. 3. The polygons represent the division of the landscape into irregular cells and the dark grey cell represents a cell that has been ignited. The cell's neighbours are those cells with a common boundary. Given the distance and direction from the centre of the cell to each of its neighbours and the rate of spread of the fire as a function of direction  $R(\theta)$ , the elapsed time between ignition of the cell and of each of the cell's neighbours is the distance divided by the directional rate of spread.

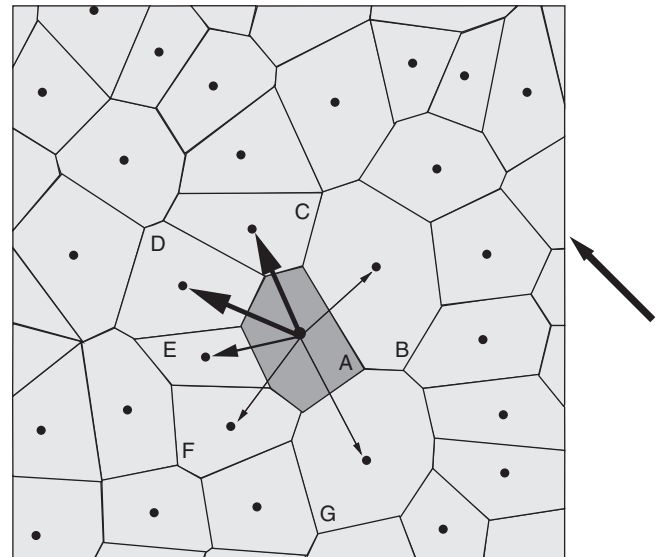


**Fig. 3.** Layout of patches showing the delay in ignition of neighbours depending on distance and direction – the thicker the line, the shorter the delay. After ignition of cell A, the neighbours are ignited later with the propagation delay influenced by the SE wind direction indicated to the side of the figure. This figure also shows the Voronoi tessellation of the points and the neighbours of Voronoi cell A are B, C, D, E, F and G.

### Discrete event simulation

Each cell has several neighbours and, if it is in the path of the fire, will receive several ignition events. The fire state behaviour diagram shown in Fig. 2 guarantees that each cell is ignited only once. To ensure that cells are ignited in the correct time sequence, each event is placed on a global event queue and is time-stamped by a future point in time when the event is scheduled to occur (Zeigler 1984). Events are ordered according to their time stamps and are processed in temporal sequence. Initially, the queue is populated with the ignition, weather and fuel moisture change events that describe where the fire starts and how the weather varies over the time of the simulated fire. When a cell enters the ignited state, ignition events are queued for all of its neighbours, to be processed after the propagation delay has elapsed. A schematic diagram of this procedure is shown in Fig. 4. This method of propagating the fire one event at a time is called discrete event simulation (Zeigler 1984) and was originally implemented for integrated circuit design but has also been employed for bushfire simulation (e.g. Muzy *et al.* 2002). It is an extremely efficient technique because the computational time is proportional to the number of cells that are ignited. In methods where the whole fire front is broken into a chain of spatial points and these are updated simultaneously, the time step must be chosen small enough to track the fastest moving part of the fire front accurately. Therefore, on the flanks of the fire where the fire moves very slowly, a large number of steps are required to move the fire over a given distance. Given that the head fire rate of spread can be up to 50 times faster than the flank rate of spread (e.g. Sneeuwjagt and Peet 1985), and that a large fraction of the fire front may be distant from the head fire, it is clear that the discrete event simulation approach is

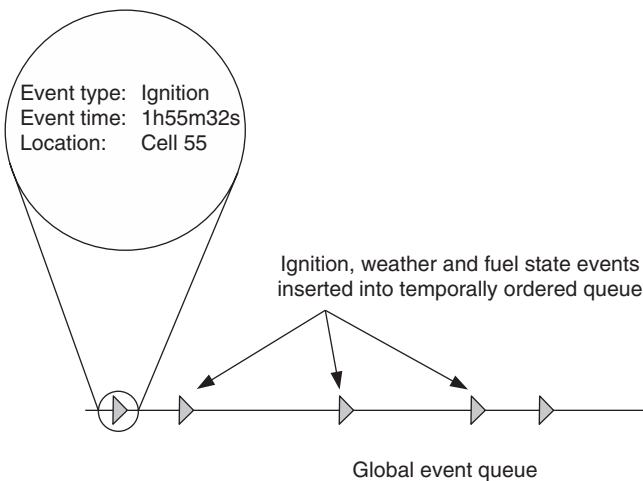


**Fig. 4.** Schematic showing queuing of ignition, fuel state and weather events onto the global event queue. The simulator removes the first event from the queue, updates cell, weather and fuel states and queues any resulting ignition events.

much faster than any method that updates the entire fire front simultaneously.

#### Cell structure

Our definition of a cell does not place any specific constraints on how cells are distributed over the landscape or even that neighbours are necessarily geographically close to each other. Traditional cellular modelling approaches divide the landscape into regular lattices for several reasons. First of all, spatial data is generally stored in a raster format, so that this format can be easily read into the simulator. Second, the calculation of the neighbourhood is extremely simple and the neighbours are the cells in the adjacent rows and columns of the array of cells. To allow arbitrary cell structures, a more sophisticated approach is required. Each cell automaton has an identifier and also stores a list of the neighbouring cell identifiers. During initiation of the simulation, the neighbourhood of each cell is calculated and accessed as required.

#### Irregular grid generation

For an arbitrary set of points on a two-dimensional landscape, the Voronoi tessellation constructs a set of polygons called Voronoi cells (e.g. Braun and Sambridge 1995). The Voronoi cell around a point contains all the area that is closer to that point than to any other. The natural neighbours of each Voronoi cell are the cells with a common boundary as pictured in Fig. 3. The Delaunay triangulation of a set of points is the dual of the Voronoi tessellation and connects each of the points to their natural neighbours. Efficient algorithms are freely available to construct the Voronoi tessellation and Delaunay triangulations of an arbitrary set of points (Barber *et al.* 1996).

As discussed in the introduction, it has been found previously (e.g. Kourtz and O'Regan 1971; Sullivan and Knight 2008) that a regular grid causes artificial distortions to the fire shapes generated by some simulators. One method that has been used

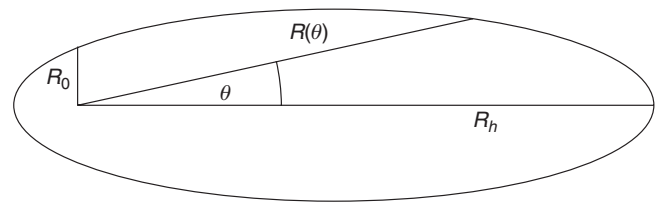


**Fig. 5.** Rate of spread as a function of direction for an elliptical fire shape.

to solve this problem is to extend the neighbourhood of each cell beyond the immediate neighbours (e.g. Kourtz and O'Regan 1971), which allows a greater freedom of choice in the direction the fire can travel, thus reducing the distortion of fire shape. This method can potentially decrease the spatial resolution because the spatial variation in fuel and topography between the ignited cell and the more distant neighbours in the extended neighbourhood are effectively ignored if the fire travels directly to the distant neighbour. In the current paper, we propose a second method, which is to use an irregular grid. Compared with the extended neighbourhood, there is not as large a choice in directions for the fire to travel from any given point on the grid, but the set of directions is different for each point on the grid.

There are several methods of distributing points on the landscape irregularly. A purely random distribution would either leave large parts of the landscape with no points or require an extremely large number of points. The Poisson disk distribution is a random set of points on the landscape, but with the additional constraint that no two points are closer than a given distance, thus ensuring a relatively uniform coverage. Such distributions can be generated efficiently (Dunbar and Humphreys 2006) and sufficient points are selected to achieve the desired spatial resolution. After generating the Poisson disk distribution points, the Voronoi diagram and Delaunay triangulation are calculated using the quickhull algorithm (Barber *et al.* 1996) to determine the polygon boundaries and neighbours of each cell. The fuel type for each cell is determined from the predominant fuel found within the cell and the slope determined from the elevation of points within or close to the cell depending on the resolution of the topography dataset. We demonstrate below that the directions to neighbours are relatively uniformly distributed, so that there is no 'preferred' grid orientation.

#### Rate of spread as a function of direction

Empirical fire behaviour meters predict the head fire rate of spread, that is, the speed with which the fire travels in the direction of the wind. Under uniform fuel and wind conditions, a fire ignited from a point forms an approximately elliptical shape with the ignition point at one of the foci of the ellipse as in Fig. 5 (e.g. Alexander 1985). Assuming an elliptical fire shape, the rate of spread in other directions is less than in the maximum spread direction and is given by the distance from the focus to the edge of the ellipse. The distance from the focus to the ellipse along the major axis is the head fire rate of spread,  $R_h$ , and the distance from the focus to the ellipse orthogonal to the major axis (*semi-latus rectum*) is the zero-wind rate of spread (i.e. the head fire rate of spread for the same conditions, but no wind),  $R_0$ .

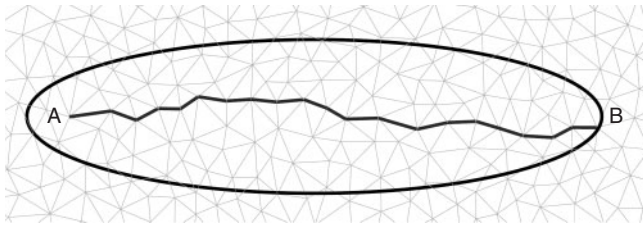


**Fig. 6.** Delaunay triangulation showing the irregular grid and the path of ignitions as a fire ignited at A spreads to point B. The length of the path is longer than the direct distance and includes segments with a variety of orientations with respect to the maximum spread direction. The ellipse shows the region that should be ignited by the time B is ignited.

The directional rate of spread at an angle  $\theta$  to the major axis is given by

$$R(\theta) = \frac{R_0}{1 - \left(1 - \frac{R_0}{R_h}\right) \cos \theta} \quad (1)$$

#### *Microscopic and macroscopic rates of spread*

Eqn 1 gives the macroscopic rate of spread required by the fire behaviour meter and used by wave front propagation schemes to determine the directional rate of spread (Anderson *et al.* 1982). By our abstraction of the landscape as a set of irregularly spaced points connected by a grid, ignitions must follow a path through this network as shown in Fig. 6. The length of the path from A to B in Fig. 6 is further than the Euclidean distance between the two points. Furthermore, the orientation of the paths includes a range of directions up to  $\sim 30^\circ$  away from the maximum spread direction, and the function in Eqn 1 decreases rapidly as  $\theta$  deviates from zero. Therefore, if we were to calculate the propagation delay between each pair of points on the path AB using the macroscopic rate of spread, it would take significantly longer for the fire to travel from A to B than the distance divided by the head fire rate of spread. For example, using Eqn 1 and  $R_h/R_0 = 20$ ,  $R(10^\circ) = 15.5R_0$ , or in other words, the directional spread rate at  $10^\circ$  from the maximum spread direction is 77% of the head fire rate of spread. As approximately two-thirds of the edges on the path AB will be oriented at an angle greater than  $10^\circ$  from the maximum spread direction, the macroscopic rate of spread when the propagation delay is calculated using Eqn 1 is less than 77% of the head fire rate of spread.

To counter this problem, we modified the microscopic rate of spread (i.e. the distance between neighbours divided by the propagation delay) and allowed the head fire rate of spread to be achieved for a larger range of directions. The microscopic rate of spread must also be increased to compensate for the fact that the distance travelled along the network is greater than the direct distance between two points. The function for the microscopic rate of spread should have the following properties:

- its value remains close to the head fire rate of spread up to around  $30^\circ$  from the maximum spread direction;
- it is a continuous function of direction;
- it is symmetric about the maximum spread direction;
- backing and flanking fires travel at the zero-wind rate of spread;

- it depends on the fire behaviour model via the head fire rate of spread and zero-wind rate of spread.

The simplest model satisfying these criteria can be described with two parameters. The first parameter of the model  $\alpha$  is defined as the direction that separates two regions: for angles greater than  $\alpha$ , the backing rate of spread is employed, whereas for angles from  $0^\circ$  to  $\alpha$ , a value between the head fire and zero-wind rate of spread is used with the maximum at  $0^\circ$ . To satisfy the first criterion above,  $\alpha > 30^\circ$ . The purpose of the second parameter,  $\beta$ , is to allow for the fact that on an irregular grid, fire cannot travel in a straight line, so that the rate of spread in all directions must be amplified. This parameter  $\beta$  is related to the geometry of the irregular grid and its Delaunay triangulation as well as the ratio  $R_h/R_0$  as is shown below. The following form for the microscopic rate of spread between adjacent nodes satisfies all the criteria above:

$$R_{micro}(\theta) = \begin{cases} (1 + \beta) \left( \frac{R_0(1 - \cos \theta) + R_h(\cos \theta - \cos \alpha)}{1 - \cos \alpha} \right), & |\theta| < \alpha \\ (1 + \beta)R_0 & |\theta| \geq \alpha \end{cases} \quad (2)$$

This function has the properties that the maximum microscopic rate of spread is at  $\theta = 0$  with a value of  $(1 + \beta)R_h$  and the rate decreases linearly as a function of  $\cos \theta$  to  $(1 + \beta)R_0$  at  $\theta = \alpha$  and beyond. We note that this function is quite different from Eqn 1. For the example given above where  $R_h/R_0 = 20$  and a value of  $\alpha = 40^\circ$ ,  $R(10^\circ) = 18.8(1 + \beta)$ , which may be greater than the head fire rate of spread, depending on the value chosen for  $\beta$ .

It remains now to determine appropriate values for  $\alpha$  and  $\beta$ . It is of prime importance that the macroscopic head fire rate of spread closely approximates  $R_h$  with small variance because this is the best constrained observation relating to fire spread. A reasonable approximation of the length-to-breadth ratio is also required; however, the data for this parameter are not as well constrained by experimental data (for example, variations in the wind direction would modify length-to-breadth ratio, but all of the data come from wildfire scars with no accurate wind measurements). The shape of fires has variously been described as elliptic, double elliptic and lemniscate (Alexander 1985) and it has been found that these shapes, or even a rectangle, provide adequate approximations to observed fire shapes (Green *et al.* 1983). Therefore, we determined the value of  $\alpha$  that provides elongated fire shapes with length-to-breadth ratios that are comparable with those for an ellipse. We then calculated the macroscopic head fire rate of spread for a range of values of  $\beta$  and  $R_h/R_0$  and inferred the value of  $\beta$  for which the macroscopic head fire rate of spread matches  $R_h$ .

We first describe our method for calculating the simulated macroscopic head fire rate of spread  $R_{h,macro}$ . The function  $R_{micro}(\theta)$  determines the propagation delay for each pair of neighbours in a connected grid like the one shown in Fig. 6 for an easterly spread direction and for a given set of values of  $(R_h, \alpha, \beta)$  with  $R_0 = 1$ . We calculated the time for a fire to travel from an ignition point near the western edge of the grid to all points in the grid (e.g. Johnson 1977). The fire arrival times are sorted in time order and each point that advances the fire

**Table 1. The macroscopic rate of spread as a function of the head fire rate of spread and  $\beta$  for the value  $\alpha = 40^\circ$** 

The value of  $\beta$  that provides the closest agreement between the macroscopic head fire rate of spread ( $R_h$ ) is shaded. The last row shows the macroscopic head fire rate of spread using Eqn 3 to calculate  $\beta$ .  $\alpha$  and  $\beta$  are defined in Eqn 2

$\beta$	$R_h$						
	1	2	5	10	20	50	100
0.00	0.962 ± 0.003	1.75 ± 0.02	4.0 ± 0.1				
0.15	1.107 ± 0.004	2.01 ± 0.03	4.6 ± 0.1	8.7 ± 0.4			
0.30			5.2 ± 0.1	9.9 ± 0.4	19 ± 1	47 ± 3	94 ± 6
0.60				12.2 ± 0.5	24 ± 1	58 ± 3	116 ± 7
Eqn 3	1.001 ± 0.003	2.00 ± 0.01	5.01 ± 0.06	10.0 ± 0.2	20.0 ± 0.5	49 ± 2	98 ± 7

front eastwards is selected (i.e. the first time the fire reaches a given distance east of the ignition). The first few points are discarded to minimise the influence of the neighbourhood of the ignition point, and ignitions after the fire reaches the easterly edge are also discarded. The easterly distance from the ignition point is plotted against time and the macroscopic head fire rate of spread is estimated as the slope of the line of least-squares fit. In order to estimate  $R_{h,macro}$  independently from ignition location, the average from 10 different ignition points is taken. The rate of increase in width of the fire and the backing rate of spread are estimated in a similar way and the length-to-breadth ratio is calculated from these values.

$R_{h,macro}$  is calculated for a range of values of ( $R_h$ ,  $\alpha$ ,  $\beta$ ) with  $R_0 = 1$  and fuel and weather uniform in space and time, in order to estimate the appropriate values  $\alpha'$  and  $\beta'$  such that  $R_{h,macro}(R_h, \alpha', \beta') \approx R_h$ . As mentioned above,  $R_{h,macro}$  is estimated by simulations from 10 ignition points to minimise the influence of the choice of ignition point and it is presented as a mean value with the standard deviation obtained from the 10 ignitions. Table 1 shows the results of these calculations with  $\alpha = 40^\circ$ . For each column of the table, the cell for which  $R_{h,macro}$  is closest to  $R_h$  is shaded. As  $R_h$  increases, a larger value of  $\beta$  is required so that the macroscopic head fire rate of spread matches  $R_h$ . For each column in Table 1, we interpolate to determine  $\beta'$  for which  $R_{h,macro}(R_h, \alpha, \beta') \approx R_h$ . We then fit a curve through the seven points to get the following relationship:

$$\beta'(R_h/R_0) = \frac{-0.42}{(R_h/R_0)^3} + \frac{0.91}{(R_h/R_0)^2} - \frac{0.84}{(R_h/R_0)} + 0.39 \quad (3)$$

Substituting this revised form for  $\beta$  into Eqn 2 and estimating  $R_{h,macro}$  as before gives an excellent fit to  $R_h$  as shown in the last row of Table 1, while the standard deviation of  $R_{h,macro}$  varies from 0.3% for  $R_h/R_0 = 1$  up to 7% for  $R_h/R_0 = 100$ . These values are much less than the deviation of fire behaviour models from the fire spread observations from which they are derived (e.g. fig. 4 of Cheney *et al.* (1998) shows a standard deviation of the misfit of observations to a fire behaviour meter of around 25%).

The same procedure has been repeated for other values of  $\alpha$  but the results have not been tabulated. Because  $\alpha$  affects the range of angles over which the head fire rate of spread is allowed, it mostly affects the lateral spread and length-to-breadth ratio of

**Table 2. Theoretical and simulated length-to-breadth ratio of fire spread**

The theoretical value is calculated for an ellipse from Eqn 4 and the simulated value is calculated for  $\alpha = 40^\circ$  and  $\beta$  calculated according to Eqn 3

$R_h/R_0$	Length-to-breadth ratio	
	Ellipse	Calculated
1	1.00	1.00 ± 0.02
2	1.15	1.41 ± 0.02
5	1.67	2.32 ± 0.05
10	2.29	3.0 ± 0.1
20	3.20	3.7 ± 0.4
50	5.03	5.5 ± 1.7
100	7.09	7.7 ± 4.3

fire. As mentioned above, the length-to-breadth ratio is not as well determined from observational data as the head fire rate of spread. Therefore the results of our simulations are compared with the length-to-breadth ratio that would be predicted for an elliptical-shaped fire, but the value of  $\alpha'$  is not formally inferred as for  $\beta'$ .

If the fire were a perfect ellipse according to Eqn 1, the length-to-breadth ratio would be:

$$(l:b)(R_h/R_0) = \frac{R_h/R_0}{\sqrt{2R_h/R_0 - 1}} \quad (4)$$

Table 2 gives a comparison of the theoretical and calculated length-to-breadth ratios for a range of values of head fire rate of spread where  $\alpha = 40^\circ$  and  $\beta$  is calculated according to Eqn 3. There is good agreement for  $R_h/R_0 > 20$ , but the fires are too narrow below this value because the zero-wind rate of spread is used for the directional rate of spread for  $\theta > \alpha$  in Eqn 2. This could be rectified by allowing  $\alpha'$  to vary as a function of  $R_h/R_0$  but we are unaware of analyses of length-to-breadth data combined with accurate wind observations that would justify this enhancement and we simply chose the value of  $\alpha$  that is a good approximation to the ellipse shape under a large range of conditions. Furthermore, when the simulator is applied to real fires, the maximum spread direction varies over time because

of wind direction variation over time and slope variation across the landscape. The change in the direction of maximum spread causes much larger changes in the directional rate of spread than allowing  $\alpha'$  to vary as a function of  $R_h/R_0$ .

For larger values of  $\alpha$ , the length-to-breadth ratio of fires did not match the elliptical approximation as well. For example, with  $\alpha = 45^\circ$ , the length-to-breadth ratio is underestimated for  $R_h/R_0 > 20$ . Smaller values of  $\alpha$  lead to greater variability in the estimate of  $R_{h,macro}$  because the most direct path in the direction of the wind contains more edges where  $R_{micro}(\theta)$  is small compared with  $R_h$ .

### *Simulator description*

The simulation consists of an initialisation phase, where static cell data such as location and fuel type are designated, followed by a simulation phase. In the initialisation phase, a set of static data is loaded into the simulator. These static data consist of the location, fuel type, fuel load and elevation of each cell, as well as a list of neighbours with which each cell interacts, and a fuel table. The fuel table lists the input parameters required for the calculation of head fire rate of spread for the given fuel type. Wind and slope contributions to the head fire rate of spread are combined by converting the slope component of the head fire rate of spread to an equivalent wind speed (i.e. the wind speed that would produce the same head fire rate of spread as on the slope in the absence of wind). The actual wind vector and equivalent wind vector due to the slope are added to determine an effective wind vector that is used as input to the fire behaviour meter.

During the simulation, dynamic data represent the state of the whole fire system being modelled. This includes the fire and fuel states of all cells, the global weather state, and an event queue, which drives the temporal evolution of the simulation. The global weather state records the current ambient (i.e. distant from any fire front) air temperature, relative humidity, wind direction and wind speed. In grass fuels, the fuel moisture can be directly calculated from the current weather. For larger fuels, the calculation of fuel moisture is more complex, so we included fuel moisture update events to allow the precalculation of fuel moisture changes outside the simulation software. At any point in time, a map can be generated showing which cells have been ignited, thus displaying the current state of the fire.

## **Results**

### *Poisson disk distribution edge properties*

In the introduction, we stated that the use of an irregular grid removes the bias introduced by regular grids. To demonstrate this property, we first show a plot of the orientations of the edges of the Delaunay triangulation of the Poisson disk distribution of points in Fig. 7. The figure shows that there is approximately the same number of edges in each direction. In contrast, a regular grid only has edges in a small finite number of directions (four, six, eight or more for larger neighbourhoods). This indicates that the length of the shortest path in any given direction on the irregular grid should be independent of the actual direction, whereas the length of the shortest path on a regular grid varies with direction.

### *Independence of rate of spread on underlying grid*

The ultimate goal of introducing the irregular grid is to produce simulated fire shapes that are independent of the orientation of the maximum spread direction. To show this independence, we calculated the macroscopic head fire rate of spread using the same method as above for all compass directions at 5-degree intervals. For each direction, the rate of spread is calculated from 10 different ignition points so that the standard deviation of macroscopic rate of spread can be estimated. The results are plotted in Fig. 8a for a head fire rate of spread ratio of  $R_h/R_0 = 50$ . The macroscopic head fire rate of spread and its variation in each direction are consistent with the fitted macroscopic rate of spread derived for spread in the easterly direction. The rate of spread is independent of the orientation of the wind.

### *Scale invariance*

Given that the propagation delay is calculated as the distance between points divided by the rate of spread, a uniform change in scale (e.g. by refining the mesh size) does not change the macroscopic rate of spread owing to the fact that the propagation delay and distance between points are scaled by the same amount. Nevertheless, it is not self-evident that spatial variation in the mesh size would produce the correct rate of spread. To confirm this property, we created a mesh with two Poisson disk distributions where the spacing for the northern half of the grid was double that of the southern half. The macroscopic head fire rate of spread was then calculated using the same method as above for a range of different directions and ignition locations. For the bi-resolution grid, the calculation of the macroscopic rate of spread as a function of direction was repeated and the results presented in Fig. 8b. The ignitions for the directions 90 to 265° are started in the coarse part of the grid, while the other ignitions are started in the fine part of the grid. The macroscopic rates of spread are statistically indistinguishable from the results for the uniform grid. A larger standard deviation is observed because the northern half of the grid is coarser than in the uniform grid.

### *Simulation performance*

Generally, it is hard to compare the computer performance of one simulator with another. Performing the same simulation on the same computer under a variety of conditions is one such test. However, the difference in speed between discrete event methods and the traditional fire front propagation methods is sufficiently large that anecdotal evidence shows the potential performance gains of using the discrete event approach. Simulation times for a real fire using *FARSITE* typically take a few minutes to run (e.g. Finney 1999) whereas the time taken for the simulations presented below is of the order of a second. This magnitude difference cannot be attributed to differences in computer power and grid resolution alone. Furthermore, part of the computational time for both simulations is taken up in generating graphics and the output of data that are not actually part of the time required for the computation. This speed-up is due to the fact that computational time increases linearly with the area ignited for the discrete event approach. For fire front propagation, computational time increases with increasing length of fire line where significant amounts of computation are required to model the dynamics of slow-moving parts of the fire and 'housekeeping'

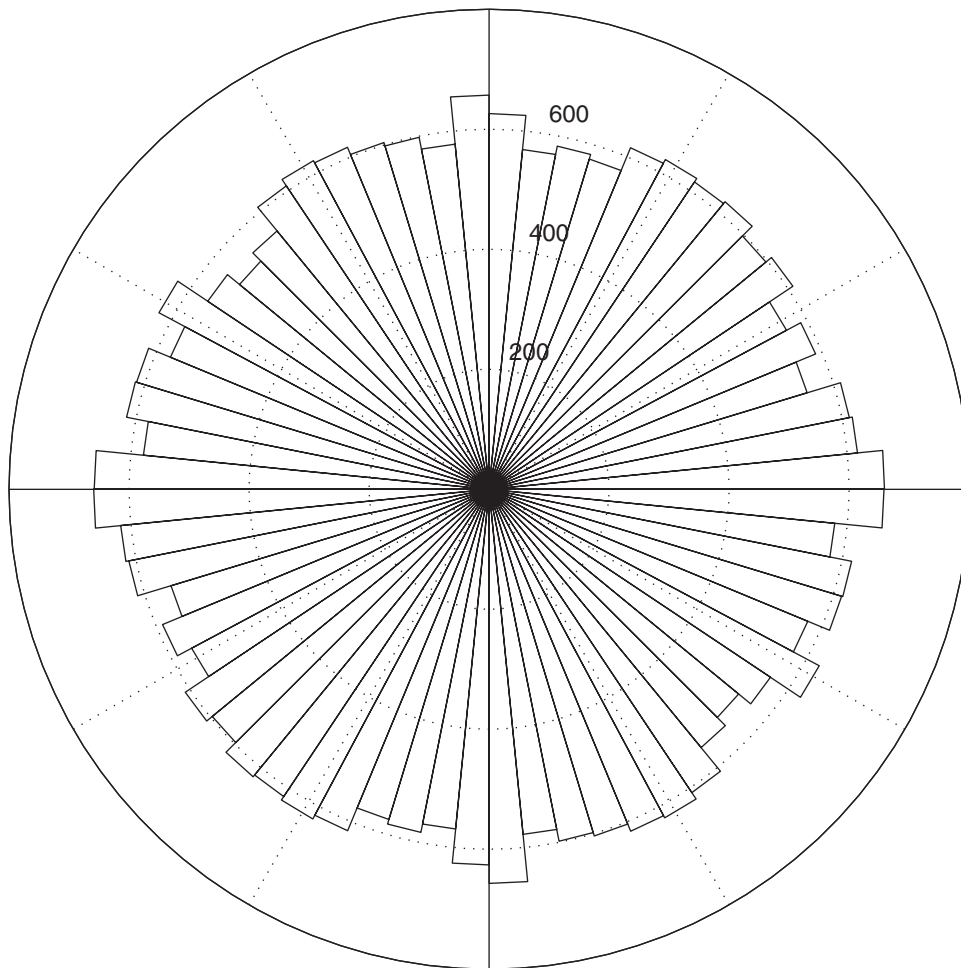


**Fig. 7.** Orientations of the 38 000 edges of the Delaunay triangulation of 6420 points of the Poisson disk distribution. This rose plot gives the frequency of edges in a given direction range. There are 64 bins and the plot is symmetric because every edge is counted twice starting from either end. With 64 bins, there are on average 601 edges per bin with a standard deviation of 30. For a regular grid with eight neighbours, all bins would be empty except those in the directions (0, 45, ..., 315). For the same number of edges as the irregular grid, the standard deviation of the bin sizes for the regular grid would be 1590 or 53 times larger than for the irregular grid.

tasks such as checking that the fire front does not overlap with itself.

#### *Fire shape for uniform wind and fuel conditions*

A series of simulation experiments are presented to demonstrate that the simulation technique presented produces realistic fire spread dynamics for a range of scenarios.

In the absence of wind, the rate of spread is the same in all directions; setting  $R_h/R_0 = 1$  in Eqn 2, the microscopic rate of spread is also uniform and 4% larger than the macroscopic rate (from Eqn 3). Fig. 9 shows a fire spreading at  $50 \text{ m h}^{-1}$  in the absence of wind with the contours showing the fire position at hourly intervals. It can be seen that the fire remains circular with the radius increasing by 50 m each hour. The irregular grid causes small random perturbations on the circular shape but no macroscopic distortion.

In the presence of wind or slope, the fire travels fastest in a particular direction where the head fire rate of spread can be

much larger than the rate in the absence of wind or slope. Observations of experimental and wild fires indicate that fire in a uniform fuel with constant wind should have an approximately elliptical shape (Alexander 1985), though other shapes such as double ellipse, ovoid or rectangle are also adequate approximations (Green *et al.* 1983). Fig. 10a shows a fire ignited from a point with a westerly wind where the head fire rate of spread is  $1000 \text{ m h}^{-1}$  while the zero-wind rate of spread is  $31 \text{ m h}^{-1}$ . The figure shows the position of the fire at 15 min intervals up to 90 min and the fire travels in an easterly direction moving forward by  $\sim 250 \text{ m}$  each 15 min. The fire also increases in width by  $\sim 60 \text{ m}$  each 15 min (note from Fig. 5 that the rate of increase in width is more than double the zero-wind rate of spread) so that the length-to-breadth ratio is  $\sim 4.2$ , which is close to the value 4.0 calculated from Eqn 4. The overall fire shape is elongated, with the widest part of the fire closer to the head fire than the ignition location. The fire contours are jagged and include small unburnt enclaves. The enclaves are caused when the neighbour

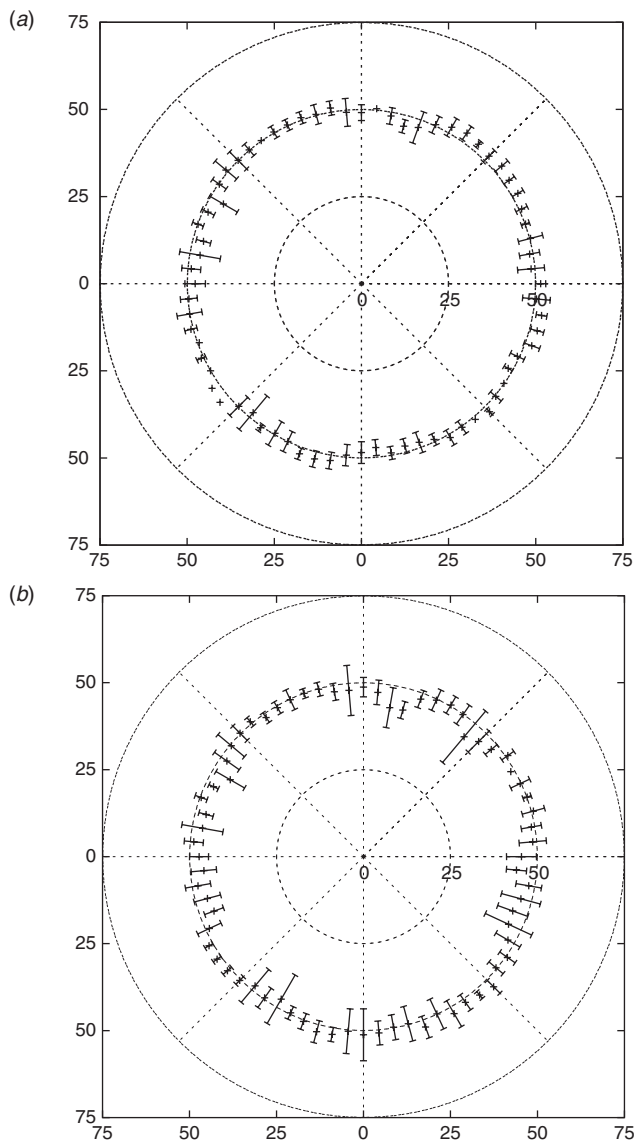


**Fig. 8.** Rate of spread as a function of direction for a head fire rate of spread of 50. The error bars represent the standard deviation of the rate of spread from 10 different ignition points for each maximum spread direction. (a) Uniform grid. (b) Grid spacing in the northern half is double that of the southern half. Using all 720 estimates of rate of spread for the uniform grid gives a head fire rate of spread of  $50.4 \pm 1.5$  and for the bi-resolution grid  $49.2 \pm 2.0$ . The increase in standard deviation is due to the overall coarser resolution of the bi-resolution grid.

closest to the downwind direction is at a significant angle from the wind direction. Therefore, the rate at which the fire moves to that neighbour is much slower than the head fire rate of spread. In the meantime, the fire continues to move downwind at the head fire rate of spread on other parts of the fire front that do have neighbours close to the downwind direction, leaving an unburnt enclave that is burnt a little later (e.g. the enclaves for the 15-min contour in Fig. 10 are not present at 30 min). The presence of these enclaves (and the jaggedness of the contours) is caused by

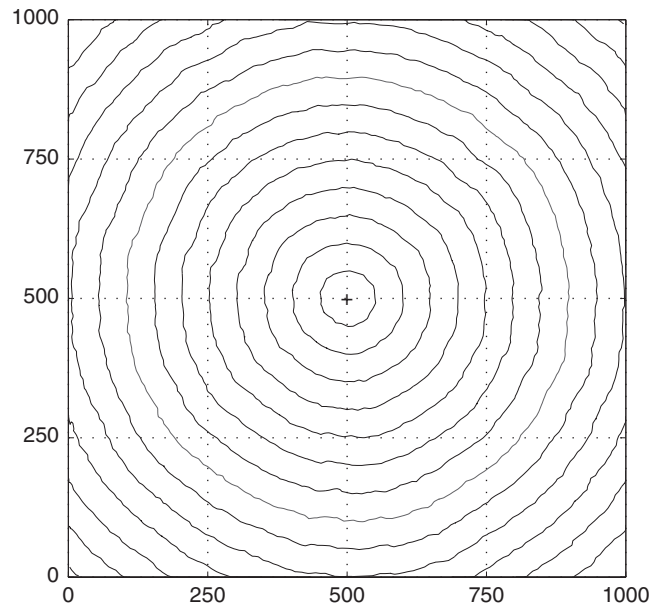


**Fig. 9.** Fire spread contours at 1-h intervals for a point fire with no wind travelling at  $50 \text{ m h}^{-1}$ . The  $x$  and  $y$  axis labels are distances in metres. The simulated fire spreads at  $\sim 50 \text{ m h}^{-1}$  equally in all directions from the ignition point marked with a plus sign (+).

the great contrast between the speed of fire propagation depending on the orientation of the edges in the neighbourhood graph with respect to the maximum spread direction. There are no enclaves in the no-wind simulation in Fig. 9 because the speed of fire propagation is uniform in all directions.

To demonstrate the effect of grid resolution on fire spread rate and shape, the same simulation is performed on a grid with double the grid spacing (i.e. half the resolution) in Fig. 10b. The forward and flank rates of spread are the same as for the finer-resolution grid but with differences in the detailed shape of the fire at any given time. The differences are caused by the different edge orientations of the two grids, and comparison of Fig. 10a and Fig. 10b shows that the rate of spread and fire shape are independent of grid resolution as also shown in Fig. 8.

As demonstrated in Fig. 8, the forward rate of spread is not artificially modified owing to the alignment of wind direction with respect to the underlying grid. We now show that fire shape is also independent of wind direction with respect to the grid. Fig. 11 shows the fire position of four fires after 90 min burning with the same head fire rate of spread as in Fig. 10 but for four different wind directions. There are minor variations in the fire shape between fires because each fire encounters different parts of the grid with different edge orientations, but the head fire travels  $\sim 1500 \text{ m}$  in each case and the width of the fire is between 300 and 350 m. The results in Fig. 11 can be compared with those in Fig. 1, which were calculated on a regular grid with the same head fire and a smaller flank fire rate of spread. For the regular grid calculation, values of  $\alpha = 60^\circ$ ,  $\beta = 0$  were employed to minimise the variation in fire shape as a function of wind direction. For either an irregular or regular grid, the neighbour in the direction that is closest to the wind direction is always the

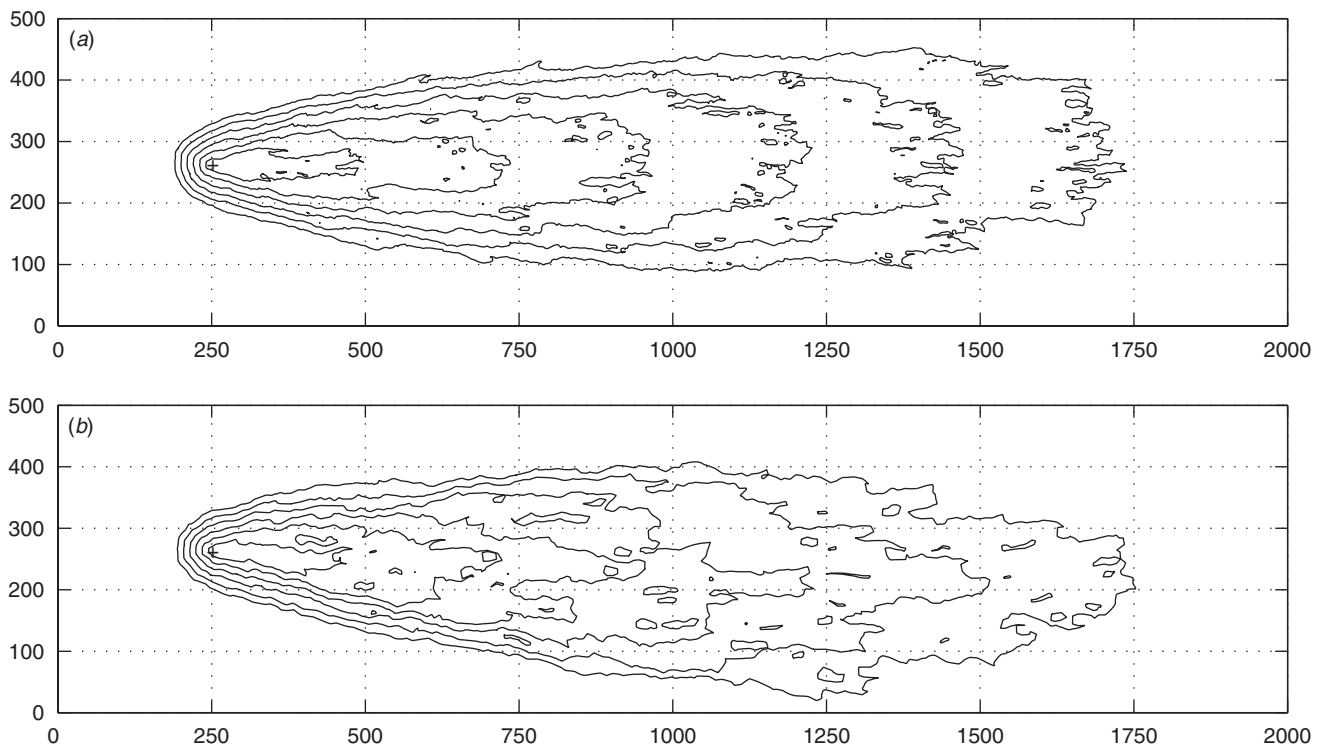


**Fig. 10.** Fire spread for a point ignition with a westerly wind where the head fire rate of spread is  $1000 \text{ m h}^{-1}$  and the zero wind rate of spread is  $31 \text{ m h}^{-1}$ . (a) grid resolution 5 m; (b) grid resolution 10 m. The fire shape is shown at 15-min intervals up to 90 min with the ignition location marked with a plus sign (+). The head fire travels  $\sim 250 \text{ m}$  during each 15-min interval. The fire increases in width by  $\sim 60 \text{ m}$  every 15 min. The overall rate of forward and flank spread for the coarser grid is the same as for the finer grid, but the randomness of the grid produces different fire boundaries at any given time.

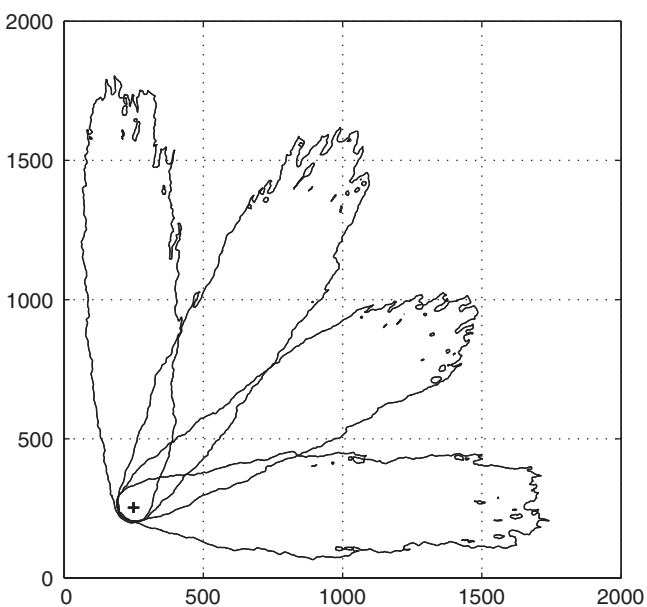


**Fig. 11.** Fire spread after 90 min for a point ignition where the head fire rate of spread is  $1000 \text{ m h}^{-1}$  and the flank fire rate of spread is  $31 \text{ m h}^{-1}$ . The fire shape is shown for four different wind directions ( $180^\circ$ ,  $210^\circ$ ,  $240^\circ$ ,  $270^\circ$ ) with the same ignition location marked with a plus sign (+). The four fires show a consistent head fire rate of spread with the fire travelling  $\sim 1500 \text{ m}$  from the ignition location with a maximum width of 300–350 m.

first ignited. The reason the distortion is so obvious on a regular grid is that this direction is the same for every cell, and the fire spreads fastest along the grid axis. For an irregular grid, the neighbour that is closest to the wind direction is equally likely to be clockwise or anticlockwise from the wind direction and therefore, over time, the fire heads in the right direction.

#### *Mt Cooke fire reconstruction*

We illustrate use of our simulator in reconstructing a historical fire where high-quality data are available. On 9 January 2003 at  $\sim 2150$  hours local time, lightning ignited a forest fire in jarrah forest near Mt Cooke, Western Australia ( $116.295^\circ \text{E}$   $32.375^\circ \text{S}$ ) and spread to around 30 ha in 8 h overnight. After 0800 hours on 10 January, fire burnt through 15-year old fuels at  $500\text{--}1000 \text{ m h}^{-1}$  under dry hot NW winds. At 1220 hours, the forward rate of spread was estimated at  $2500 \text{ m h}^{-1}$  with spotting 1–2 km ahead of the main front. A spot fire (at  $116.359^\circ \text{E}$   $32.476^\circ \text{S}$ )  $\sim 6 \text{ km}$  ahead of the fire front started around 1200 hours and the wind direction swung around to the west. The fire eventually ran into 5-year old fuels at 0500 hours the following morning and with the reduced fire intensity due to the lighter fuel loads and more benign conditions, firefighters were able to suppress the head fire at this time. Fire was contained on the NE flank because prescribed burning the previous year left little fuel to burn, resulting in a low fire intensity, which was easily suppressed, whereas spot fires ahead of the main fire ignited in 7-year old fuels were not able to be

## MOUNT COOKE FIRE, WESTERN AUSTRALIA 9–11 JANUARY 2003

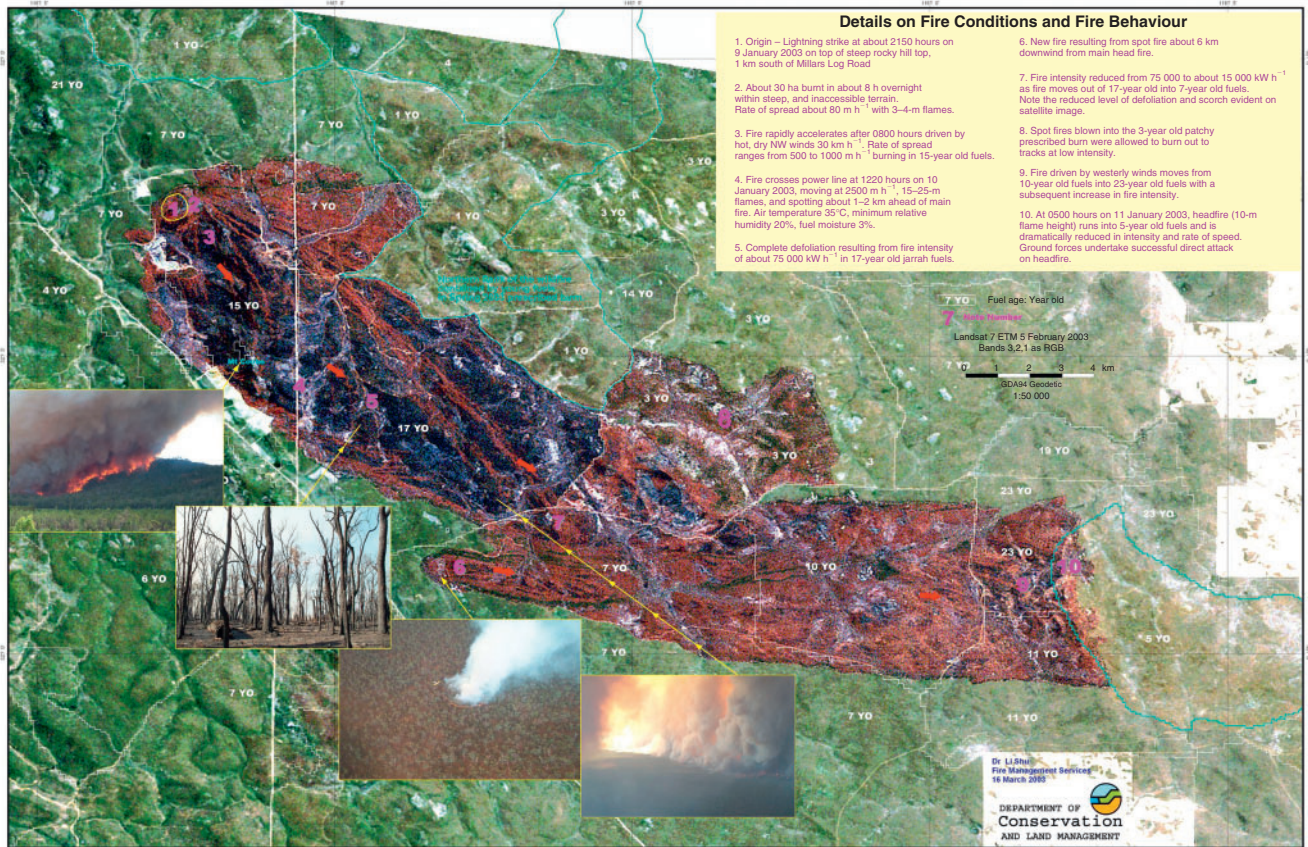


**Fig. 12.** Satellite image of the fire scar from the Mt Cooke fire (9–11 January 2003), which started in the NW in 15-year old fuels at 2150 hours on 9 January, travelled SE into 17-year old fuel crossing the powerline (N–S line at left) at 1220 hours, ignited a spot fire at 1200 hours (central south) and headed easterly in the afternoon before being extinguished in 5-year old fuel at 0500 hours on 11 January. The burnt-out region in 3-year old fuels on the central northern flank was due to spotting and was not suppressed to allow fuel reduction. Image taken from a poster by L. Shu, Department of Environment and Conservation, Western Australia.

contained by aerial suppression. A map of the burnt area is shown in Fig. 12. Topography for the region is from Geoscience Australia's 9<sup>th</sup> topographic database (GEODATA 9 Second DEM Version 2.1, [http://www.ga.gov.au/nmd/products/digidat/dem\\_9s.htm](http://www.ga.gov.au/nmd/products/digidat/dem_9s.htm), accessed 28 July 2008).

The Forest Fire Behaviour Tables for Western Australia (Sneeuwjagt and Peet 1985) were used to calculate the head fire rate of spread as a function of fuel moisture, wind, slope and fuel load in jarrah fuels. The temperature, relative humidity and rainfall data from the nearby Bickley (116.137°E 32.008°S) weather station were used to estimate the fine fuel moisture according to the model of Matthews (2006). Hourly wind data were also obtained from the same location, but the wind directions did not coincide with those experienced on the fire ground as indicated by the direction of fire spread. Therefore, a simple wind model was adopted assuming a wind direction of 330° before 0800 hours on 10 January, changing to 300° at 0800 hours and changing to 280° at 1200 hours. The combination of wind speed and fire behaviour model underpredicted the area burnt, and to fit the observed rate of spread of the fire, the wind speed was increased by a constant factor of 1.6. The Forest Fire Behaviour Tables require the observed wind to be reduced by a factor of 2 to

6 depending on the height at which the wind speed is measured and the local topography. Originally the wind speed was reduced by a factor of 3; so, in effect, the wind reduction factor is 2. This smaller reduction factor could be attributed to a more open forest, difference in wind speed between the weather station and the fire ground, or underprediction by the fire spread meter under extreme conditions. Because of the small amount of fire growth overnight, the fire was assumed to be ignited at 0400 hours on 10 January and finished burning at 2100 hours.

The Forest Fire Behaviour Tables predict that head fire spread rate is strongly dependent on fuel load, so that for the conditions experienced in the Mt Cooke fire, the head fire rate of spread is reduced to 0.2 of the standard rate of spread for 3-year old fuel, while it is increased by 2.7 for 17-year old fuels, i.e. under the same conditions, the head fire rate of spread is 10 times faster in the old fuels than in the young fuels. As a consequence of this, it was found that the area burnt was very sensitive to the wind scale factor. A smaller value than the one we used would have resulted in the fire failing to travel far enough south to reach the 7-year old fuels by the time of the westerly wind change and a much reduced area being burnt. Fig. 13a shows hourly contours of the fire position derived from the ignition, weather,

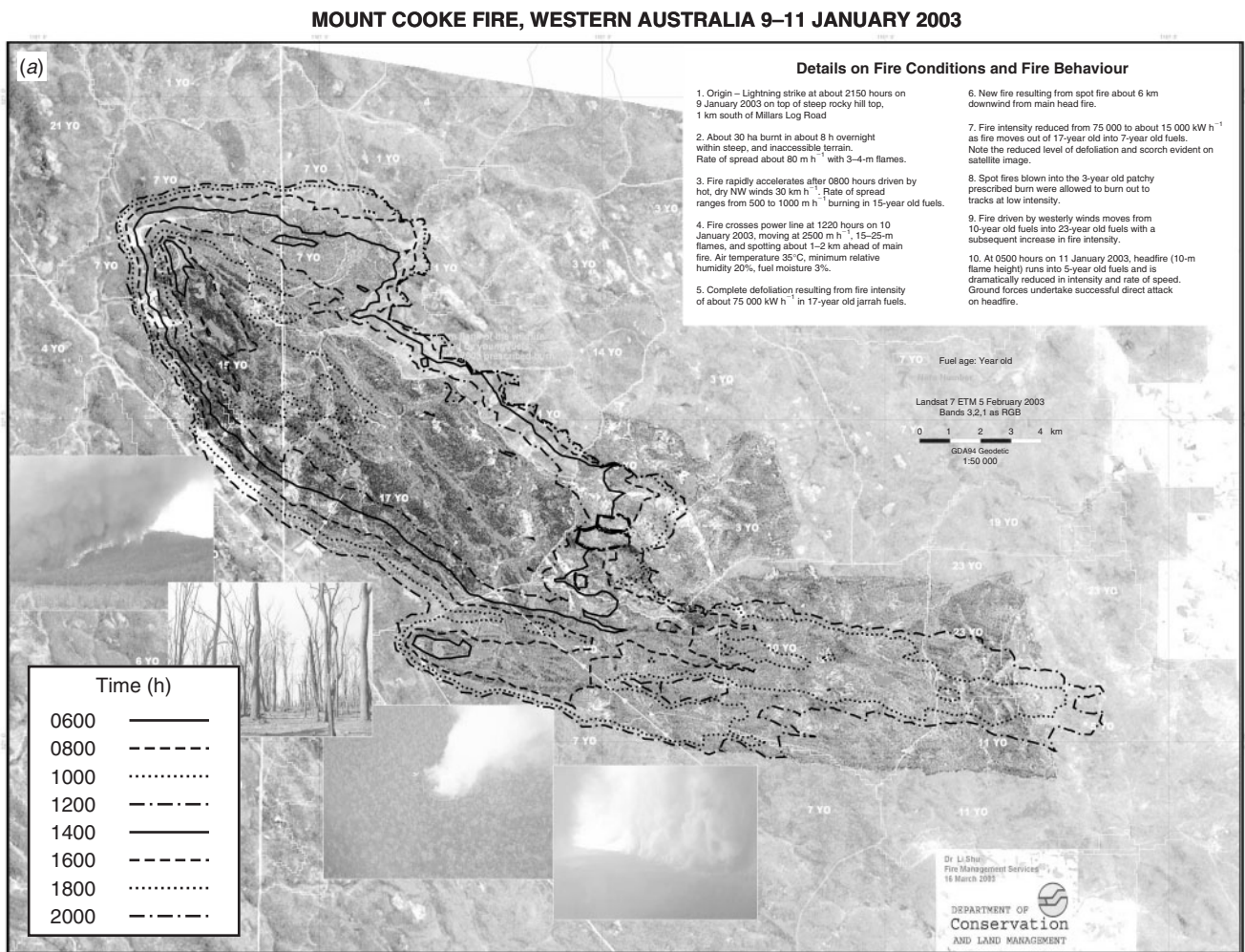


**Fig. 13.** Two-hourly fire position from simulation of the Mt Cooke fire. (a) With fuel ages as recorded by Department of Environment and Conservation, Western Australia; (b) with a uniform fuel age of 15 years. Original image was modified from a poster by L. Shu, Department of Environment and Conservation, Western Australia.

topography, fuel and fire behaviour model using the simulation and also seeded with the spot fire ignition at 1200 hours on 11 January. The only part of the fire scar that does not match well is the area on the northern flank that was ignited by spotting and not surface fire. The grid spacing used in the simulation is 200 m, resulting in a grid of  $\sim 14\,000$  points. The simulation took 1.3 s including the time required for graphics output on a desktop personal computer with a 3.2 GHz processor.

A potential use for simulation is to evaluate different fuel, weather and suppression scenarios and to help inform policy on fire prevention. In Western Australia, there is a strong program of prescribed burning in the southern forests as evidenced by the large areas around Mt Cooke that had been burnt in the previous 3 years. We can estimate the effect of the fire modelled previously if no prescribed burning program had occurred by assuming that no fires had burnt for the past 15 years. Fig. 13b shows the resulting fire, which is much larger than the one that actually occurred; it would have been difficult to suppress owing to the higher fuel loads and consequent fire intensity.

## Discussion

Cell-based methods of fire spread simulation have long been viewed with distrust because of the distortion of the fire shape they cause, despite the benefits of increased performance and ease of implementation. The distortion is caused by the fact that the fire always spreads to the neighbour that is closest to the downwind direction. For a regular grid and constant wind direction, this is always in the same direction, resulting in a fire that spreads fastest along the grid axis instead of in the direction of the wind. Our implementation of a cell-based simulator with an irregular grid addresses this problem and results in fire spread that more closely approximates the elongated fire shape observed in fire experiments. This is due to the fact that the neighbour that is closest to the downwind direction may be on either side of the wind direction and, over time, the fire spreads in the direction of the wind independently of the underlying grid. Overcoming the distortion as found in other cell-based simulation methods enables the use of efficient discrete event simulation with its enhanced performance and opens up the possibility of running

## MOUNT COOKE FIRE, WESTERN AUSTRALIA 9–11 JANUARY 2003

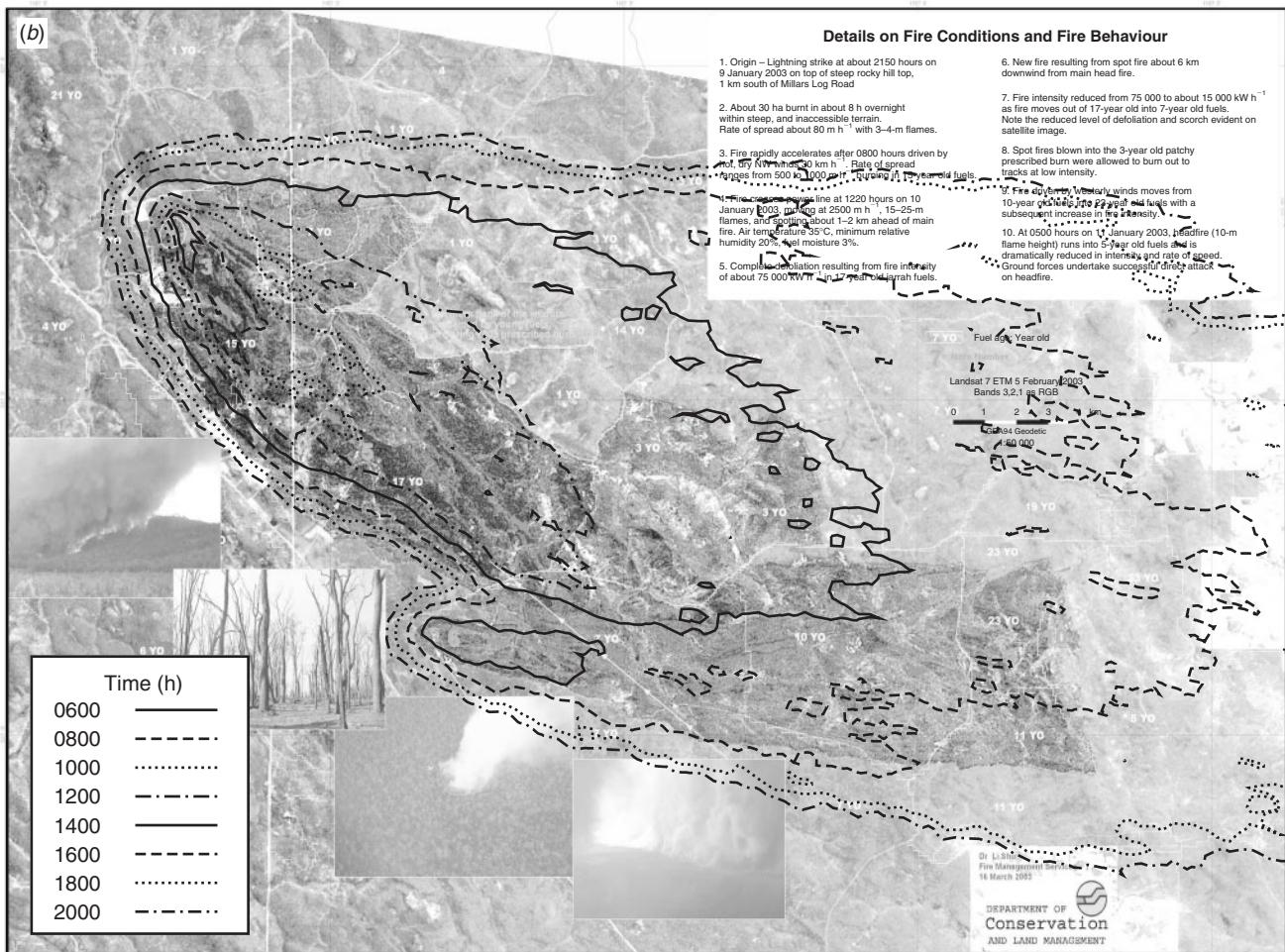


Fig. 13. (Continued)

large numbers of simulations on the same fire under different weather forecast scenarios to determine probable fire behaviour. The simulator could thus be used in estimating fire risk by simulating fire dynamics under a range of weather scenarios and ignition locations.

Implementation of the irregular grid is possible by making the neighbourhood of each cell explicit. The Poisson disk distribution of points is chosen for the location of points so that the edge directions between neighbouring points are uniformly distributed, while the distance between points is within a narrow range. Tests under ideal scenarios with an absence of wind or uniform wind demonstrate that such simulations produce the correct head fire rates of spread and acceptable length-to-breadth ratios. The implementation on an irregular grid requires a microscopic rate of spread function (Eqn 2) that is different from the macroscopic directional rate of spread with two parameters inferred to ensure that the fire simulations behave correctly. If observational data require a better fit to the length-to-breadth ratio, this could be obtained by allowing  $\alpha$  to depend on the ratio of head fire to zero-wind rate of spread. Also, the irregular grid can produce small regions that do not get burnt until some time after the

passing of the fire front and an irregular fire front owing to the large contrast between the speed of fire propagation depending on the orientation of the edges in the neighbourhood graph with respect to the maximum spread direction.

We have demonstrated the use of the simulator on a historical forest fire in Western Australia, achieving an excellent agreement between simulated and actual fire following a slight modification of the input data. We have also given an indication of possible uses of the simulator, for example, to examine how the progress of the fire depends on input parameters such as the initial fuel load. The high performance of the simulator enhances the user's ability to test a larger range of inputs owing to the rapid calculation of simulation results.

### Acknowledgements

Li Shu, Lachlan McCaw and Rick Sneeuwjagt of the Department of Environment and Conservation, Western Australia, are thanked for weather, fuel and fire data for the Mt Cooke fire. Thanks to Jim Gould, Neil Burrows and two anonymous reviewers for reviews of an earlier version of the present paper. This research has been funded in part by the Australian Bushfire Cooperative

Research Centre. Support from the National Information and Communications Technology Australia (NICTA) Centre of Excellence to G. J. Milne in the form of a NICTA Fellowship is also gratefully acknowledged.

## References

- Alexander ME (1985) Estimating the length-to-breadth ratio of elliptical forest fire patterns. In 'Proceedings of the Eighth National Conference on Fire and Forest Meteorology', 29 April–2 May 1985, Detroit, MI, pp. 287–304. (Society of American Foresters: Bethesda, MD)
- Anderson DH, Catchpole EA, De Mestre NJ, Parkes T (1982) Modelling the spread of grass fires. *Journal of the Australian Mathematical Society B* **23**, 451–466.
- Barber CB, Dobkin DP, Huhdanpaa H (1996) The quickhull algorithm for convex hulls. *ACM Transactions on Mathematical Software* **22**, 469–483. doi:10.1145/235815.235821
- Berjak SG, Hearne JW (2002) An improved cellular automaton model for simulating fire in a spatially heterogeneous savanna system. *Ecological Modelling* **148**, 133–151. doi:10.1016/S0304-3800(01)00423-9
- Braun J, Sambridge M (1995) A numerical method for solving partial differential equations on highly irregular evolving grids. *Nature* **376**, 655–660. doi:10.1038/376655A0
- Cheney NP, Gould JS (1995) Fire growth in grassland fuels. *International Journal of Wildland Fire* **5**, 237–247. doi:10.1071/WF9950237
- Cheney NP, Gould JS, Catchpole WR (1998) Prediction of fire spread in grasslands. *International Journal of Wildland Fire* **8**, 1–13. doi:10.1071/WF9980001
- Coleman J, Sullivan A (1996) A real-time computer application for the prediction of fire spread across the Australian landscape. *Simulation* **67**, 230–240. doi:10.1177/003754979606700402
- CWFGM Project Steering Committee (2004) 'Prometheus User Manual ver. 3.0.1.' (Alberta Sustainable Resource Development: Edmonton, AB, Canada)
- Dunbar D, Humphreys G (2006) A spatial data structure for fast Poisson-disk sample generation. *ACM Transactions on Graphics* **25**, 503–508. doi:10.1145/1141911.1141915
- Finney MA (1998) FARSITE: Fire Area Simulator – model development and evaluation. USDA Forest Service, Rocky Mountain Research Station, Research Paper RMRS-RP-004. (Ogden, UT)
- Finney MA (1999) Mechanistic modelling of landscape fire patterns. In 'Spatial Modelling of Forest Landscape Change: Approaches and Applications'. (Eds DJ Mladenhoff, WL Baker) pp. 186–209. (Cambridge University Press: New York)
- Green DG, Gill AM, Noble IR (1983) Fire shapes and the adequacy of fire spread models. *Ecological Modelling* **20**, 33–45. doi:10.1016/0304-3800(83)90030-3
- Green DG, Tridgell A, Gill AM (1990) Interactive simulation of bushfires in heterogeneous fuels. *Mathematical and Computer Modelling* **13**, 57–66. doi:10.1016/0895-7177(90)90099-9
- Johnson DB (1977) Efficient algorithms for shortest paths in sparse networks. *Journal of the ACM* **24**, 1–13. doi:10.1145/321992.321993
- Kourtz P, O'Regan W (1971) A model for a small forest fire to simulate burned and burning areas for use in a detection model. *Forest Science* **17**, 163–169.
- Linn R, Riesner J, Colman JJ, Winterkamp J (2002) Studying wildfire behaviour using FIRETEC. *International Journal of Wildland Fire* **11**, 233–246. doi:10.1071/WF02007
- Matthews S (2006) A process-based model of fine fuel moisture. *International Journal of Wildland Fire* **15**, 155–168. doi:10.1071/WF05063
- McArthur AG (1967) Fire Behaviour in Eucalypt Forests. Department of National Development Forestry and Timber Bureau, Leaflet No 107. (Canberra)
- McDaniel J (2007) Calculated risk. *Wildfire* **16**(2). Available at [http://wildfiremag.com/mag/calculated\\_risk](http://wildfiremag.com/mag/calculated_risk) [Verified 29 July 2008]
- Muzy A, Innocenti E, Aiello A, Santucci J-F, Wainer G (2002) Cell-DEVS quantization techniques in a fire spreading application. In 'Proceedings of the 2002 Winter Simulation Conference', 8–11 December 2002, San Diego, CA. (Eds E Yücesan, C-H Chen, JL Snowdon, JM Charnes) pp. 542–549. (IEEE Computer Society: Washington, DC)
- Pastor E, Zarate L, Planas E, Arnaldos J (2003) Mathematical models and calculation systems for the study of wildland fire behaviour. *Progress in Energy and Combustion Science* **29**, 139–153. doi:10.1016/S0360-1285(03)00017-0
- Richards GD (1999) The mathematical modelling and computer simulation of wildland fire perimeter growth over a 3-dimensional surface. *International Journal of Wildland Fire* **9**, 213–221. doi:10.1071/WF00019
- Sneeuwjagt RJ, Peet GB (1985) 'Forest Fire Behaviour Tables for Western Australia.' (Department of Conservation and Land Management: Perth)
- Sullivan AL (2008) Wildland surface fire spread modelling, 1990–2007. 3: Simulation and mathematical analogue models. *International Journal of Wildland Fire*, in press. doi:10.1071/WF06144
- Sullivan AL, Knight IK (2001) Estimating error in wind speed measurements for experimental fires. *Canadian Journal of Forest Research* **31**, 401–409. doi:10.1139/CJFR-31-3-401
- Sullivan AL, Knight IK (2008) A hybrid cellular automata/semi-physical model of fire growth. *Complexity International* **12**, msid09. Available at <http://www.complexity.org.au/ci/vol12/msid09/> [Verified 20 August 2008]
- Zeigler BP (1984) 'Multifaceted Modelling and Discrete Event Simulation.' (Academic Press: London)

Manuscript received 1 November 2006, accepted 17 March 2008